

# A CONVERGENT FINITE VOLUME SCHEME FOR DIFFUSION ON EVOLVING SURFACES

MARTIN LENZ\*, SIMPLICE FIRMIN NEMADJIEU†, AND MARTIN RUMPF‡

**Abstract.** A finite volume scheme for transport and diffusion problems on evolving hypersurfaces is discussed. The underlying motion is assumed to be described by a fixed, not necessarily normal, velocity field. The ingredients of the numerical method are an approximation of the family of surfaces by a family of interpolating simplicial meshes, where grid vertices move on motion trajectories, a consistent finite volume discretization of the induced transport on the simplices, and a proper incorporation of a diffusive flux balance at simplicial faces. The semi-implicit scheme is derived via a discretization of the underlying conservation law, and discrete counterparts of continuous a priori estimates in this geometric setup are proved. The continuous solution on the continuous family of evolving surfaces is compared to the finite volume solution on the discrete sequence of simplicial surfaces and convergence of the family of discrete solutions on successively refined meshes is proved under suitable assumptions on the geometry and the discrete meshes. Furthermore, numerical results show remarkable aspects of transport and diffusion phenomena on evolving surfaces and experimentally reflect the established convergence results. Finally, we discuss how to combine the presented scheme with a corresponding finite volume scheme for advective transport on the surface via an operator splitting and present some applications.

**Key words.** Finite volume method, evolving surfaces, transport diffusion equations

**AMS subject classifications.** 35K57, 58J35, 65M12, 65M15, 74H15, 76E06, 76M12.

**1. Introduction.** In many applications in materials science, biology and geometric modeling evolution problems do not reside on a flat Euclidean domain but on a curved hypersurface. Frequently this surface is itself evolving in time driven by some velocity field. In general the induced transport is not normal to the surface but incorporates tangential motion of the geometry and thus a corresponding tangential advection process on the evolving surface. In [10] Dziuk and Elliot proposed a finite element scheme for the numerical simulation of diffusion processes on such evolving surfaces. In this paper we pick up the finite volume methodology introduced by Eymard, Gallouët and Herbin in [13] on fixed Euclidean domains and discuss a generalization in case of transport and diffusion processes on curved and evolving surfaces<sup>1</sup>. The general motivation for a finite volume formulation is the potential of a further extension to coupled diffusion and dominating nonlinear advection models. Here, we restrict to linear transport.

Applications of the considered model are the diffusion of densities on biological membranes or reaction diffusion equations for texture generation on surfaces [21]. Frequently, partial differential equations on the surface are coupled to the evolution of the geometry itself. Examples are the spreading of thin liquid films or coatings on surfaces [20], transport and diffusion of a surfactant on interfaces in multiphase flow [17], surfactant driven thin film flow [15] on the enclosed surface of lung alveoli coupled with the expansion or contraction of the alveoli, and diffusion induced grain boundary motion [3]. In this paper, we suppose the evolution of the surface to be given a priori and study the finite volume discretization of diffusion on the resulting

---

\*University of Bonn, Germany, ([martin.lenz@ins.uni-bonn.de](mailto:martin.lenz@ins.uni-bonn.de))

†University of Bonn, Germany, ([simplice.nemadjieu@ins.uni-bonn.de](mailto:simplice.nemadjieu@ins.uni-bonn.de))

‡University of Bonn, Germany, ([martin.rumpf@ins.uni-bonn.de](mailto:martin.rumpf@ins.uni-bonn.de))

<sup>1</sup>A preliminary form of this paper was published in an 8 page conference proceedings: *M. Lenz, S. Nemadjieu, M. Rumpf*, “Finite Volume Method on Moving Surfaces”, *5th International Symposium on Finite Volumes for Complex Applications*, 2008.

family of evolving surfaces as a model problem. The evolving surfaces are discretized by simplicial meshes, where grid nodes are assumed to be transported along motion trajectories of the underlying flow field. The approach applies to evolving polygonal curves and triangulated surfaces. In the presentation we focus on the case of moving two-dimensional surfaces. Finite volume methods on curved geometries have been discussed recently in [4, 8], but to the best of our knowledge they have so far not been analysed on evolving surfaces.

An alternative approach would be to consider a level set representation via an evolving level set function. In this case, projections of the derivatives onto the embedded tangent space provide a mechanism for computing geometric differential operators [1] on fixed level set surfaces. Finite elements in this context are discussed in [2] and a narrow band approach with a very thin fitted mesh is presented in [7], and in [14] an improved approximation of tangential differential operators is presented. Furthermore, in [11] a finite element level set method is introduced for the solution of parabolic PDEs on a family of evolving implicit surfaces.

Our finite volume method is closely related to the finite element approach by Dziuk and Elliott [10]. They consider a moving triangulation, where the nodes are propagating with the actual motion velocity, which effectively leads to space time finite element basis functions similar to the ELLAM approach [16]. We consider as well a family of triangulated surfaces with nodes located on motion trajectories where the triangles are treated as finite volume cells. The resulting scheme immediately incorporates mass conservation. An overview on computational approaches which use moving meshes to solve PDEs is given in [18]. Here, the moving mesh reflects the Eulerian coordinates underlying the evolution problem but on a fixed computational domain.

The paper is organized as follows. In Section 2 the mathematical model is discussed and in Section 3 we derive the finite volume scheme on simplicial grids. Discrete a priori estimates consistently formulated in terms of the evolving geometry are established in Section 4. In Section 5 we state and prove the main convergence result. Finally, Section 6 discusses an operator splitting scheme for the coupling of diffusive and advective transport so far not encoded in the surface motion itself and in Section 7 numerical results are presented.

**2. Mathematical model.** We consider a family of compact, smooth, and oriented hypersurfaces  $\Gamma(t) \subset \mathbb{R}^n$  ( $n = 2, 3$ ) for  $t \in [0, t_{max}]$  generated by an evolution  $\Phi : [0, t_{max}] \times \Gamma_0 \rightarrow \mathbb{R}^n$  defined on a reference surface  $\Gamma_0$  with  $\Phi(t, \Gamma_0) = \Gamma(t)$ . Let us assume that  $\Gamma_0$  is  $C^3$  smooth and that  $\Phi \in C^1([0, t_{max}], C^3(\Gamma_0))$ . For simplicity we assume the reference surface  $\Gamma_0$  to coincide with the initial surface  $\Gamma(0)$  (cf. Figure 5.2).

We denote by  $v = \partial_t \Phi$  the velocity of material points and assume the decomposition  $v = v_n \nu + v_{tgl}$  into a scalar normal velocity  $v_n$  in direction of the surface normal  $\nu$  and a tangential velocity  $v_{tgl}$ . The evolution of a conservative material quantity  $u$  with  $u(t, \cdot) : \Gamma(t) \rightarrow \mathbb{R}$ , which is propagated with the surface and simultaneously undergoes a linear diffusion on the surface, is governed by the parabolic equation

$$\dot{u} + u \nabla_\Gamma \cdot v - \nabla_\Gamma \cdot (\mathcal{D} \nabla_\Gamma u) = g \quad \text{on } \Gamma = \Gamma(t), \quad (2.1)$$

where  $\dot{u} = \frac{d}{dt} u(t, x(t))$  is the (advective) material derivative of  $u$ ,  $\nabla_\Gamma \cdot v$  the surface divergence of the vector field  $v$ ,  $\nabla_\Gamma u$  the surface gradient of the scalar field  $u$ ,  $g$  a source term with  $g(t, \cdot) : \Gamma(t) \rightarrow \mathbb{R}$  and  $\mathcal{D}$  a diffusion tensor on the tangent bundle. Here we assume a symmetric, uniformly coercive  $C^2$  diffusion tensor field on whole

$\mathbb{R}^n$  to be given, whose restriction on the tangent plane is then effectively incorporated in the model. With a slight misuse of notation, we denote this global tensor field also by  $\mathcal{D}$ . Furthermore, we impose an initial condition  $u(0, \cdot) = u_0$  at time 0. Let us assume that the mappings  $(t, x) \rightarrow u(t, \Phi(t, x))$ ,  $v(t, \Phi(t, x))$ , and  $g(t, \Phi(t, x))$  are  $C^1([0, t_{max}], C^3(\Gamma_0))$ ,  $C^0([0, t_{max}], C^3(\Gamma_0))$  and  $C^1([0, t_{max}], C^1(\Gamma_0))$  regular, respectively. For the ease of presentation we restrict here to the case of a closed surface without boundary. Our results can easily be generalized to surfaces with boundary, on which we either impose Dirichlet or Neumann boundary condition. For a discussion of existence, uniqueness and regularity of solutions we refer to [10] and the references therein.

**3. Derivation of the finite volume scheme.** For the ease of presentation we restrict ourselves to the case of two dimensional surfaces in  $\mathbb{R}^3$ . A generalization of the numerical analysis presented here is straightforward. We consider a sequence of regular surface triangulations  $\{\Gamma_h^k\}_{k=0, \dots, k_{max}}$  with  $\Gamma_h^k$  interpolating  $\Gamma(t_k)$  for  $t_k = k\tau$  and  $k_{max}\tau = t_{max}$  (cf. Dziuk and Elliott [10] for the same set up with respect to a finite element discretization). Here,  $h$  indicates the maximal diameter of a triangle on the whole sequence of triangulations,  $\tau$  the time step size and  $k$  the index of a time step. All triangulations share the same grid topology, and given the set of vertices  $x_j^0$  on the initial triangular surface  $\Gamma_h^0$  the vertices of  $\Gamma_h^k$  lie on motion trajectories. Thus, they are evaluated based on the flux function  $\Phi$ , i. e.  $x_j(t_k) = \Phi(t_k, x_j^0)$  (cf. Figure 3.1). Single closed triangles or edges of the topological grid  $\Gamma_h$  are denoted by  $S$  and  $\sigma$ , respectively. Upper indices denote the explicit geometric realization at the corresponding time step.

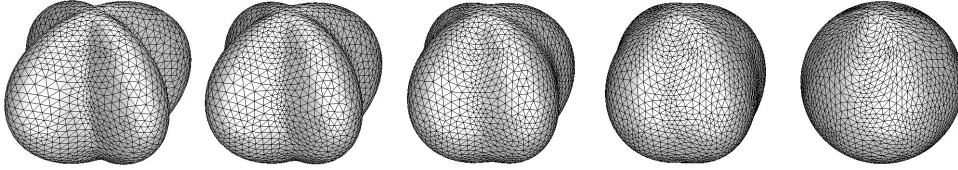


FIGURE 3.1. Sequence of triangulations  $\Gamma_h^k$  interpolating a four-fold symmetric object in its evolution.

Thus, a closed triangle of the triangulated surface geometry  $\Gamma_h^k$  is denoted by  $S^k$ . We assume that the triangulations  $\Gamma_h^k$  are regular, i. e. there exist constants  $c, C > 0$  such that  $ch^2 \leq m_S^k \leq Ch^2$  for all  $S$  and all  $k$ , where  $m_S^k$  denotes the area of  $S^k$ . As in the Euclidean case discussed in [13] we also assume that for all time steps  $t_k$  where  $k = 0, \dots, k_{max}$  and all simplices  $S^k \subset \Gamma_h^k$  there exists a point  $X_S^k \in S^k$  and for each edge  $\sigma^k \subset \partial S^k$  a point  $X_\sigma^k \in \sigma^k$  such that the vector  $\overrightarrow{X_S^k X_\sigma^k}$  is perpendicular to  $\sigma^k$  with respect to the scalar product induced by the inverse of the diffusion tensor on the triangle  $S^k$  at the point  $X_\sigma^k$ , i.e.

$$(\mathcal{D}(X_\sigma^k))^{-1}(X_S^k - X_\sigma^k) \cdot V = 0, \quad (3.1)$$

where  $V$  is a vector parallel to the edge  $\sigma^k$ . Furthermore, we assume that these points can be chosen such that for two adjacent simplices  $S^k$  and  $L^k$  the corresponding points on the common edge  $\sigma^k = S^k \cap L^k$  coincide (cf. Figure 3.2). The point  $X_S^{k+1}$  at the following time step need not be the consistently transported point  $X_S^k$  under the flow  $\Phi$ . It will turn out that for the error analysis the later stated condition (5.1) is

sufficient. This allows to choose the points  $X_S^k$  in a way that fulfills these requirements without changing the grid topology between time steps, as described in the paragraph after equation (5.1).

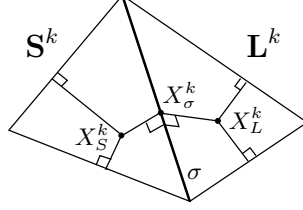


FIGURE 3.2. A sketch of the local configuration of points  $X_S^k$ ,  $X_L^k$ , and  $X_\sigma^k$  on two adjacent simplices  $S^k$  and  $L^k$ , which in general do not lie in the same plane.

For a later comparison of discrete quantities on the triangulation  $\Gamma_h^k$  and continuous quantities on  $\Gamma(t_k)$  we define a lifting operator from  $\Gamma_h^k$  onto  $\Gamma(t_k)$  via the orthogonal projection  $\mathcal{P}^k$  onto  $\Gamma(t_k)$  in direction of the surface normal  $\nu$  of  $\Gamma(t_k)$ . For sufficiently small  $h$  this projection is uniquely defined and smooth; we also assume it to be bijective. By  $S^{l,k} := \mathcal{P}^k S^k$  we define the projection of a triangle  $S^k$  on  $\Gamma(t_k)$  and by  $S^{l,k}(t) := \Phi(t, \Phi^{-1}(t_k, S^{l,k}))$  the temporal evolution of  $S^{l,k}$ , which we will take into account for  $t \in [t_k, t_{k+1}]$ . Furthermore, we can estimate the relative change of area of triangles by  $m_S^{k+1} = m_S^k (1 + O(\tau))$  for all simplices  $S^k$  and all  $k$  because of the smoothness of the flux function  $\Phi$ .

Based on these notational preliminaries we can now derive a suitable finite volume discretization. Thus, let us integrate (2.1) on  $\{(t, x) \mid t \in [t_k, t_{k+1}], x \in S^{l,k}(t)\}$ .

$$\int_{t_k}^{t_{k+1}} \int_{S^{l,k}(t)} g \, da \, dt \approx \tau m_S^{k+1} G_S^{k+1}, \quad (3.2)$$

where  $G_S^{k+1} = g(t_{k+1}, \mathcal{P}^{k+1} X_S^{k+1})$ . Using the Leibniz formula  $\frac{d}{dt} \int_{S^{l,k}(t)} u \, da = \int_{S^{l,k}(t)} \dot{u} + u \nabla_\Gamma \cdot v \, da$  (cf. [10]), we obtain for the material derivative

$$\begin{aligned} \int_{t_k}^{t_{k+1}} \int_{S^{l,k}(t)} \dot{u} + u \nabla_\Gamma \cdot v \, da \, dt &= \int_{S^{l,k}(t_{k+1})} u \, da - \int_{S^{l,k}(t_k)} u \, da \\ &\approx m_S^{k+1} u(t_{k+1}, \mathcal{P}^{k+1} X_S^{k+1}) - m_S^k u(t_k, \mathcal{P}^k X_S^k). \end{aligned} \quad (3.3)$$

Next, integrating the elliptic term again over the temporal evolution of a lifted triangular patch and applying Gauss's theorem we derive the following approximation:

$$\begin{aligned} \int_{t_k}^{t_{k+1}} \int_{S^{l,k}(t)} \nabla_\Gamma \cdot (\mathcal{D} \nabla_\Gamma u) \, da \, dt &= \int_{t_k}^{t_{k+1}} \int_{\partial S^{l,k}(t)} \mathcal{D} \nabla_\Gamma u \cdot \mu_{\partial S^{l,k}(t)} \, dl \, dt \quad (3.4) \\ &\approx \tau \sum_{\sigma \subset \partial S} m_\sigma^{k+1} \lambda_{S|\sigma}^{k+1} \frac{u(t_{k+1}, \mathcal{P}^{k+1} X_\sigma^{k+1}) - u(t_k, \mathcal{P}^k X_S^k)}{d_{S|\sigma}^{k+1}}, \end{aligned}$$

where  $\mu_{\partial S^{l,k}(t)}$  is the outer co-normal on  $\partial S^{l,k}(t)$  tangential to  $\Gamma(t)$ ,  $\sigma^{k+1}$  an edge of  $S^{k+1}$ ,  $m_\sigma^{k+1}$  the length of  $\sigma^{k+1}$ ,  $d_{S|\sigma}^{k+1} := \|X_S^{k+1} - X_\sigma^{k+1}\|$ , and  $\lambda_{S|\sigma}^{k+1} := \|\mathcal{D}_{S|\sigma}^{k+1} \mu_{S|\sigma}^{k+1}\|$ .

The discrete diffusion tensor is defined by  $\mathcal{D}_{S|\sigma}^{k+1} := (P_S^{k+1})^T \mathcal{D}(X_\sigma^{k+1}) P_S^{k+1}$ , where  $P_S^{k+1}$  is the orthogonal projection onto the plane given by  $S^{k+1}$ , and  $\mu_{S|\sigma}^{k+1}$  is the outer co-normal to  $S^{k+1}$  on the edge  $\sigma$ . Indeed, the orthogonality assumption (3.1) implies that  $(X_\sigma^{k+1} - X_S^{k+1})$  is parallel to  $\mathcal{D}_{S|\sigma}^{k+1} \mu_{S|\sigma}^{k+1}$ . Hence,  $\nabla_\Gamma u \cdot \mu_{\partial S^{l,k}(t)}$  can consistently be approximated by the difference quotient  $\lambda_{S|\sigma}^{k+1} \frac{u(t_{k+1}, \mathcal{P}^{k+1} X_\sigma^{k+1}) - u(t_{k+1}, \mathcal{P}^{k+1} X_S^{k+1})}{d_{S|\sigma}^{k+1}}$ .

Alternatively, one could introduce a diffusion tensor  $\mathcal{D}_S^{k+1} := (P_S^{k+1})^T \mathcal{D}(X_S^{k+1}) P_S^{k+1}$  on triangles and modify (3.1) and the definition of  $\lambda_{S|\sigma}^{k+1}$  accordingly. We will comment on this alternative approach in the context of the convergence analysis in Section 5.2.

Now, we introduce discrete degrees of freedom  $U_S^k$  and  $U_\sigma^k$  for  $u(\mathcal{P}^k X_S^k)$  and  $u(\mathcal{P}^k X_\sigma^k)$ , respectively. The values  $U_S^k$  are the actual degrees of freedom; they will be compiled into a function  $U^k$  that is constant on each cell  $S^k$  and is an element of the discrete solution space  $\mathcal{V}_h^k$  which is defined in (3.7) below. The  $U_\sigma^k$  are only auxiliary degrees of freedom, cf. (3.5). Then the discrete counterpart of the continuous flux balance

$$\int_{S^{l,k}(t) \cap L^{l,k}(t)} (\mathcal{D} \nabla_\Gamma u)|_{S^{l,k}(t)} \cdot \mu_{\partial S^{l,k}(t)} \, da = - \int_{S^{l,k}(t) \cap L^{l,k}(t)} (\mathcal{D} \nabla_\Gamma u)|_{L^{l,k}(t)} \cdot \mu_{\partial L^{l,k}(t)} \, da$$

on  $S^{l,k}(t) \cap L^{l,k}(t)$  for two adjacent simplices  $S^k$  and  $L^k$  is given by

$$m_\sigma^{k+1} \frac{U_\sigma^{k+1} - U_S^{k+1}}{d_{S|\sigma}^{k+1}} \lambda_{S|\sigma}^{k+1} = -m_\sigma^{k+1} \frac{U_\sigma^{k+1} - U_L^{k+1}}{d_{L|\sigma}^{k+1}} \lambda_{L|\sigma}^{k+1}$$

for the edge  $\sigma^k = S^k \cap L^k$ . Let us emphasize that this flux balance holds independently of the tilt of  $S^k$  and  $L^k$  at  $\sigma^k$ . Hence, we can cancel out the degrees of freedom

$$U_\sigma^{k+1} = \frac{U_S^{k+1} d_{L|\sigma}^k \lambda_{S|\sigma}^k + U_L^{k+1} d_{S|\sigma}^k \lambda_{L|\sigma}^k}{d_{L|\sigma}^k \lambda_{S|\sigma}^k + d_{S|\sigma}^k \lambda_{L|\sigma}^k} \quad (3.5)$$

on edges and based on the approximations for the parabolic term in (3.3) and the elliptic term in (3.4), we finally obtain the finite volume scheme

$$m_S^{k+1} U_S^{k+1} - m_S^k U_S^k - \tau \sum_{\sigma \subset \partial S} m_\sigma^{k+1} \mathcal{M}_\sigma^{k+1} \frac{U_L^{k+1} - U_S^{k+1}}{d_{S|L}^{k+1}} = \tau m_S^{k+1} G_S^{k+1}, \quad (3.6)$$

$$\text{where } \mathcal{M}_\sigma^k := \frac{\lambda_{S|\sigma}^k \lambda_{L|\sigma}^k d_{S|L}^k}{d_{L|\sigma}^k \lambda_{S|\sigma}^k + d_{S|\sigma}^k \lambda_{L|\sigma}^k}, \quad d_{S|L}^k := d_{S|\sigma}^k + d_{L|\sigma}^k.$$

This requires the solution of a linear system of equations for the cell-wise solution values  $U_S^{k+1}$  for  $k = 0, \dots, k_{max} - 1$  and for given initial data  $U_S^0$  at time  $t_0 = 0$ .

REMARK. Different from the finite volume method on Euclidean domains in [13] all coefficients depend on the geometric evolution, and thus in particular change in time. A comparison of the discrete and continuous solution requires a mapping from the sequence of triangulations  $\{\Gamma_h^k\}$  onto the continuous family of surfaces  $\{\Gamma(t)\}_{t \in [0, t_{max}]}$ .

Figure 3.3 shows two different triangulations of a (rotating) torus (cf. Figure 7.2, 7.3 and 7.4 below for corresponding numerical results). In the first case the underlying

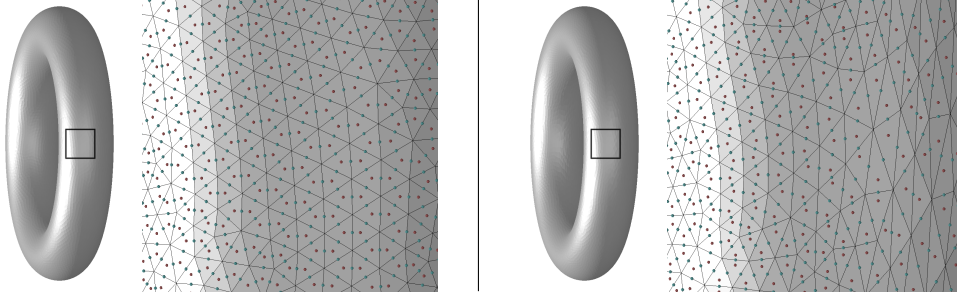


FIGURE 3.3. On the left an isotropic mesh for a torus is shown together with a zoom in with indicated points  $X_S^k$  on the triangles and  $X_\sigma^k$  on edges. On the right an anisotropic mesh corresponding to an anisotropic diffusion tensor  $\mathcal{D} = \text{diag}(\frac{1}{25}, 1, 1)$  is rendered together with the corresponding zoom. One observes in the blow up of the anisotropic mesh geometry a transition from the strongly anisotropic regime close to the center plane of the torus on the right and the more isotropic mesh on the left.

diffusion is isotropic, hence an isotropic mesh is used for the simulation of the evolution problem. In the second case an anisotropic diffusion tensor  $\mathcal{D} = \text{diag}(\frac{1}{25}, 1, 1)$  is taken into account. To enable the definition of consistent triangle nodes  $X_S^k$  and edge nodes  $X_\sigma^k$ , an anisotropic mesh has been generated. Even though  $\mathcal{D}$  is constant on  $\mathbb{R}^{3,3}$  the induced tangential diffusivity varies on the surface. This variation is properly reflected by the generated mesh. We refer to Section 7 for some remarks on the mesh generation.

Let us associate with the components  $U_S^k$  on the simplices  $S^k$  of the triangulation  $\Gamma_h^k$  a piecewise constant function  $U^k$  with  $U^k|_{S^k} = U_S^k$  and let

$$\mathcal{V}_h^k := \left\{ U^k : \Gamma_h^k \rightarrow \mathbb{R} \mid U^k|_{S^k} = \text{const} \ \forall S^k \subset \Gamma_h^k \right\} \quad (3.7)$$

be the space of these functions on  $\Gamma_h^k$ . Analogously, we denote by  $G^k$  the corresponding piecewise constant function with  $G^k|_{S^k} = G_S^k$ . On the function space  $\mathcal{V}_h^k$ , we can define a discrete energy semi norm based on a weighted sum of squared difference quotients:

DEFINITION 3.1 (Discrete energy semi norm). For  $U^k \in \mathcal{V}_h^k$  we define

$$\|U^k\|_{1, \Gamma_h^k} := \left( \sum_{\sigma=S \cap L} m_\sigma^k \mathcal{M}_\sigma^k \frac{(U_L^k - U_S^k)^2}{d_{S|L}^k} \right)^{\frac{1}{2}}. \quad (3.8)$$

Before we prove suitable a priori estimates, let us verify existence and uniqueness of the discrete solution.

PROPOSITION 3.2. The discrete problem (3.6) has a unique solution.

PROOF: The system (3.6) has a unique solution  $U^{k+1}$ , if the kernel of the corresponding linear operator is trivial. To prove this, we assume  $U^k \equiv 0$  and  $G^{k+1} \equiv 0$  in (3.6); then multiply each equation by the the corresponding  $U_S^{k+1}$  for the triangle  $S^{k+1} \subset \Gamma_h^{k+1}$ . Summing up over all simplices and taking into account the symmetry

of the second term in (3.6) with respect to the two simplices  $S^k$  and  $L^k$  intersecting at the edge  $\sigma^{k+1} = S^{k+1} \cap L^{k+1}$  we obtain

$$\|U^{k+1}\|_{L^2(\Gamma_h^{k+1})}^2 + \tau \|U^{k+1}\|_{1,\Gamma_h^{k+1}}^2 = 0,$$

from which  $U^{k+1} = 0$  follows immediately.  $\square$

Indeed, Proposition 3.2 is a direct consequence of Theorem 4.1 to be proved in the next section.

**4. A priori estimates.** In what follows we will prove discrete counterparts of continuous a priori estimates. They are related to the discrete energy estimates given in [13] in the case of finite volume methods on fixed Euclidean domains.

**THEOREM 4.1** (discrete  $L^\infty(L^2)$ ,  $L^2(H^1)$  energy estimate). *Let  $\{U^k\}_{k=1,\dots,k_{max}}$  be the discrete solution of (3.6) for given discrete initial data  $U^0 \in \mathcal{V}_h^0$ , then there exists a constant  $C$  depending solely on  $t_{max}$ , such that*

$$\max_{k=1,\dots,k_{max}} \|U^k\|_{L^2(\Gamma_h^k)}^2 + \sum_{k=1}^{k_{max}} \tau \|U^k\|_{1,\Gamma_h^k}^2 \leq C \left( \|U^0\|_{L^2(\Gamma_h^0)}^2 + \tau \sum_{k=1}^{k_{max}} \|G^k\|_{L^2}^2 \right). \quad (4.1)$$

**PROOF:** As in the proof of Proposition 3.2, we multiply the equation (3.6) by  $U_S^{k+1}$  for every cell  $S^k \in \Gamma_h^k$ , and sum over all  $S^k \in \Gamma_h^k$  to obtain (again using the symmetry of the second term in (3.6))

$$\begin{aligned} & \sum_S \left( m_S^{k+1} (U_S^{k+1})^2 - m_S^k U_S^k U_S^{k+1} \right) + \tau \sum_{\sigma=S \cap L} m_\sigma^{k+1} \mathcal{M}_\sigma^{k+1} \frac{(U_L^{k+1} - U_S^{k+1})^2}{d_{S|L}^{k+1}} \\ &= \tau \sum_S m_S^{k+1} G_S^{k+1} U_S^{k+1}, \end{aligned} \quad (4.2)$$

which leads to

$$\begin{aligned} & \|U^{k+1}\|_{L^2(\Gamma_h^{k+1})}^2 + \tau \|U^{k+1}\|_{1,\Gamma_h^{k+1}}^2 \\ & \leq \|U^k\|_{L^2(\Gamma_h^k)} \max_S \left( \frac{m_S^k}{m_S^{k+1}} \right)^{\frac{1}{2}} \|U^{k+1}\|_{L^2(\Gamma_h^{k+1})} + \tau \|G^{k+1}\|_{L^2(\Gamma_h^{k+1})} \|U^{k+1}\|_{L^2(\Gamma_h^{k+1})}. \end{aligned}$$

Then, by Young's inequality and the estimate  $\max_k \max_S \left| \frac{m_S^k}{m_S^{k+1}} - 1 \right| \leq C\tau$ , one obtains

$$\begin{aligned} & \frac{1}{2} \|U^{k+1}\|_{L^2(\Gamma_h^{k+1})}^2 + \tau \|U^{k+1}\|_{1,\Gamma_h^{k+1}}^2 \\ & \leq \frac{1}{2} \|U^k\|_{L^2(\Gamma_h^k)}^2 + \frac{C}{2} \tau \|U^{k+1}\|_{L^2(\Gamma_h^{k+1})}^2 + \frac{1}{2} \tau \|G^{k+1}\|_{L^2(\Gamma_h^{k+1})}^2. \end{aligned} \quad (4.3)$$

Using the notation  $a_k = \|U^k\|_{L^2(\Gamma_h^k)}^2$  and  $b_k = \|G^k\|_{L^2(\Gamma_h^k)}^2$ , one can deduce from  $a_k \leq a_{k-1} + C\tau a_k + \tau b_k$  that

$$a_k \leq (1 - C\tau)^{-1} (a_{k-1} + \tau b_k) \leq \dots \leq (1 - C\tau)^{-k} (a_0 + \tau \sum_{j=1}^k b_j).$$

Since

$$(1 - C\tau)^{-k} = \left( \left( 1 - \frac{Ct_k}{k} \right)^{-\frac{k}{Ct_k}} \right)^{Ct_k}$$

is bounded from above by  $2e^{Ct_k}$  for sufficiently small  $\tau$ , we immediately get the desired bound for  $\|U^k\|_{L^2(\Gamma_h^k)}^2$ :

$$\|U^k\|_{L^2(\Gamma_h^k)}^2 \leq 2e^{Ct_k} \left( \|U^0\|_{L^2(\Gamma_h^0)}^2 + \tau \sum_{j=1}^k \|G^j\|_{L^2}^2 \right).$$

We sum (4.3) over  $k = 0, \dots, k_{max} - 1$  and compensate the terms  $\|U^k\|_{L^2(\Gamma_h^k)}^2$  on the right hand side for  $k = 1, \dots, k_{max} - 1$  with those on the left, and using the already established estimate for the  $L^2$ -norm gives the bound for  $\sum_{k=1}^{k_{max}} \tau \|U^k\|_{1, \Gamma_h^k}^2$ .  $\square$

**THEOREM 4.2** (discrete  $H^1(L^2)$ ,  $L^\infty(H^1)$  energy estimate). *Let  $\{U^k\}_{k=1, \dots, k_{max}}$  be the discrete solution of (4.2) with given initial data  $U^0$ , then there exist a constant  $C$ , such that*

$$\begin{aligned} \sum_{k=1}^{k_{max}} \tau \|\partial_t^r U^k\|_{L^2(\Gamma_h^k)}^2 + \max_{k=1, \dots, k_{max}} \|U^k\|_{1, \Gamma_h^k}^2 \\ \leq C \left( \|U^0\|_{L^2(\Gamma_h^0)}^2 + \|U^0\|_{1, \Gamma_h^0}^2 + \tau \sum_{k=1}^{k_{max}} \|G^k\|_{L^2(\Gamma_h^k)}^2 \right), \end{aligned} \quad (4.4)$$

where  $\partial_t^r U^k := \frac{U^k - U^{k-1}}{\tau}$  is defined as a difference quotient in time.

**PROOF:** We multiply (3.6) by  $\partial_t^r U^{k+1}$  for every triangle  $S^k \in \Gamma_h^k$  and sum over all simplices to obtain

$$\begin{aligned} \tau \sum_S m_S^{k+1} \left( \frac{U_S^{k+1} - U_S^k}{\tau} \right)^2 \\ + \sum_{\sigma=S \cap L} m_\sigma^{k+1} \mathcal{M}_\sigma^{k+1} \left( d_{S|L}^{k+1} \left( \frac{U_L^{k+1} - U_S^{k+1}}{d_{S|L}^{k+1}} \right)^2 - \left( \frac{U_S^{k+1} - U_L^{k+1}}{d_{S|L}^{k+1}} \right) (U_S^k - U_L^k) \right) \\ = \sum_S (m_S^k - m_S^{k+1}) U_S^k \left( \frac{U_S^{k+1} - U_S^k}{\tau} \right) + \tau \sum_S m_S^{k+1} G_S^{k+1} \left( \frac{U_S^{k+1} - U_S^k}{\tau} \right). \end{aligned}$$

Using the notation

$$\begin{aligned} a_{S|L}^k &:= \sqrt{d_{S|L}^k m_\sigma^k \mathcal{M}_\sigma^k} \left( \frac{U_S^k - U_L^k}{d_{S|L}^k} \right), \quad b_S^{k+1} := \sqrt{m_S^{k+1}} \left( \frac{U_S^{k+1} - U_S^k}{\tau} \right), \\ c_{S|L}^k &:= \sqrt{\frac{d_{S|L}^k m_\sigma^{k+1} \mathcal{M}_\sigma^{k+1}}{d_{S|L}^{k+1} m_\sigma^k \mathcal{M}_\sigma^k}}, \end{aligned}$$



this can be written as

$$\begin{aligned} & \tau \sum_S (b_S^{k+1})^2 + \sum_{\sigma=S \cap L} \left( (a_{S|L}^{k+1})^2 - a_{S|L}^{k+1} c_{S|L}^k a_{S|L}^k \right) \\ &= \sum_S \left( \frac{m_S^k}{m_S^{k+1}} - 1 \right) \frac{\sqrt{m_S^{k+1}}}{\sqrt{m_S^k}} \sqrt{m_S^k} U_S^k b_S^{k+1} + \tau \sum_S \sqrt{m_S^{k+1}} G_S^{k+1} b_S^{k+1}. \end{aligned}$$

Noting that

$$(a_{S|L}^{k+1})^2 - a_{S|L}^{k+1} c_{S|L}^k a_{S|L}^k \geq \frac{1}{2} \left( (a_{S|L}^{k+1})^2 - (a_{S|L}^k)^2 \right) + (1 - c_{S|L}^k) \left( \frac{(a_{S|L}^{k+1})^2}{2} + \frac{(a_{S|L}^k)^2}{2} \right)$$

and

$$\sum_{\sigma=S \cap L} (a_{S|L}^k)^2 = \|U^k\|_{1, \Gamma_h^k}^2, \quad \sum_S (b_S^k)^2 = \|\partial_t^\tau U^{k+1}\|_{L^2(\Gamma_h^{k+1})}^2,$$

we apply Cauchy's and Young's inequality and we finally obtain

$$\begin{aligned} & \tau \|\partial_t^\tau U^{k+1}\|_{L^2(\Gamma_h^{k+1})}^2 + \frac{1}{2} \|U^{k+1}\|_{1, \Gamma_h^{k+1}}^2 - \frac{1}{2} \|U^k\|_{1, \Gamma_h^k}^2 \\ & \leq C\tau \left( \|U^{k+1}\|_{1, \Gamma_h^{k+1}}^2 + \|U^k\|_{1, \Gamma_h^k}^2 \right. \\ & \quad \left. + (\|U^k\|_{L^2(\Gamma_h^k)} + \|G^{k+1}\|_{L^2(\Gamma_h^{k+1})}) \|\partial_t^\tau U^{k+1}\|_{L^2(\Gamma_h^{k+1})} \right). \quad (4.5) \end{aligned}$$

Here, we have taken into account that  $|1 - c_{S|L}^k| \leq C\tau$  and  $\left| 1 - \frac{m_S^k}{m_S^{k+1}} \right| \frac{\sqrt{m_S^{k+1}}}{\sqrt{m_S^k}} \leq C\tau$ . Next, as in Theorem 4.1 we apply Young's inequality, sum over all time steps and obtain

$$\begin{aligned} & \sum_{k=1}^{k_{max}} \left( \frac{\tau}{2} \|\partial_t^\tau U^k\|_{L^2(\Gamma_h^k)}^2 + \frac{1}{2} \|U^k\|_{1, \Gamma_h^k}^2 - \frac{1}{2} \|U^0\|_{1, \Gamma_h^0}^2 \right) \\ & \leq \frac{C}{2} \tau \sum_{k=1}^{k_{max}} \left( \|U^k\|_{1, \Gamma_h^k}^2 + \|U^{k-1}\|_{1, \Gamma_h^{k-1}}^2 + \|U^{k-1}\|_{L^2(\Gamma_h^{k-1})}^2 + \|G^k\|_{L^2(\Gamma_h^k)}^2 \right). \quad (4.6) \end{aligned}$$

Finally, an application of Theorem 4.1 leads us to the desired estimate.  $\square$

**5. Convergence.** In this section we will prove an error estimate for the finite volume solution  $U^k \in \mathcal{V}_h^k$ . At first, we have to state how to compare a discrete solution defined on the sequence of triangulations  $\Gamma_h^k$  and the continuous solution defined on the evolving family of smooth surfaces  $\Gamma(t)$ . Here, we will take into account the lifting operator from the discrete surfaces  $\Gamma_h^k$  onto the continuous surfaces  $\Gamma(t_k)$  already introduced in Section 3. As for the error analysis of a finite element approach in [10] we use a pull back from the continuous surface onto a corresponding triangulation to compare the continuous solution  $u(t_k)$  at time  $t_k$  with the discrete solution  $U^k = \sum_S U_S^k \chi_{S^k}$ , where  $\chi_{S^k}$  indicates the characteristic function of the triangle  $S^k$ . In explicit, we consider the pull back of the continuous solution  $u$  at time  $t_k$  under this

lift  $u^{-l}(t_k, X_S^k) := u(t_k, \mathcal{P}^k(X_S^k))$  and investigate the error  $u^{-l}(t_k, X_S^k) - U_S^k$  at the cell nodes  $X_S^k$  as the value of a piecewise constant error function on the associated cells  $S^k$ .

Obviously, the consistency of the scheme depends on the behavior of the mesh during the evolution and a proper, in particular time coherent choice of the nodes  $X_S^k$ . Let us assume that

$$|\Upsilon^{k,k+1}(X_S^k) - X_S^{k+1}| \leq Ch\tau, \quad (5.1)$$

where  $\Upsilon^{k,k+1}(X_S^k)$  denotes the point on  $S^{k+1}$  with the same barycentric coordinates on  $S^{k+1}$  as the node  $X_S^k$  on  $S^k$ . (cf. (5.4) below). This condition is obviously true for  $X_S^k$  being the orthocenter of  $S^k$ , which is admissible for  $\mathcal{D} = \text{Id}$  on acute meshes. In case of an anisotropic diffusivity or non acute meshes, one chooses nodes  $X_S^k$  close to the barycenters in the least square sense, given the orthogonality relation (3.1). Algorithmically, a mesh optimization strategy enables a corresponding choice of nodes (cf. Section 7).

Finally, the following convergence theorem holds:

**THEOREM 5.1** (error estimate). *Suppose that the assumptions listed in Section 2 and 3 and in (5.1) hold and define the piecewise constant error functional on  $\Gamma_h^k$  for  $k = 1, \dots, k_{max}$*

$$E^k := \sum_S (u^{-l}(t_k, X_S^k) - U_S^k) \chi_{S^k}$$

measuring the defect between the pull back  $u^{-l}(t_k, \cdot)$  of the continuous solution  $u(t_k, \cdot)$  of (2.1) at time  $t_k$  and the finite volume solution  $U^k$  of (3.6). Thus, the error function  $E^k$  is actually an element of the same space  $\mathcal{V}_h^k$  of piecewise constant functions on  $\Gamma_h^k$  as the discrete solutions  $U^k$ , cf. (3.7). Furthermore, let us assume that  $\|E^0\|_{L^2(\Gamma_h^k)} \leq Ch$ , then the error estimate

$$\max_{k=1, \dots, k_{max}} \|E^k\|_{L^2(\Gamma_h^k)}^2 + \tau \sum_{k=1}^{k_{max}} \|E^k\|_{1, \Gamma_h^k}^2 \leq C(h + \tau)^2 \quad (5.2)$$

holds for a constant  $C$  depending on the regularity assumptions and the time  $t_{max}$ .

This error estimate is a generalization of the estimate given in [13], where the same type of first order convergence with respect to the time step size and the grid size are established for a finite volume scheme on a fixed planar domain. As usual in the context of finite volume schemes the convergence proof is based on consistency estimates for the difference terms in the discrete scheme (3.6). In the context of evolving surfaces considered here, these consistency errors significantly rely on geometric approximation estimates. Thus, in the next Paragraph 5.1 we first investigate a set of relevant geometric estimates. Afterwards, in Paragraph 5.2 these estimates will be used to establish suitable consistency results. Finally, the actual convergence result is established in Paragraph 5.3.

**5.1. Geometric approximation estimates.** In this paragraph, we first extend the definition of the projection  $\mathcal{P}^k$  to a time continuous operator  $\mathcal{P}(t, \cdot)$  which, for each  $t \in [0, t_{max}]$ , projects points orthogonally onto  $\Gamma(t)$  (cf. Figure 5.1). This operator is well defined in a neighborhood of  $\Gamma(t)$ .

We denote by  $p_0, p_1, p_2$  the vertices of a triangle  $S^k$ , and we consider  $\xi_0(x), \xi_1(x), \xi_2(x)$  the barycentric coordinates of a point  $x$  on  $S^k$ , i. e.  $x = \xi_0(x)p_0 + \xi_1(x)p_1 +$

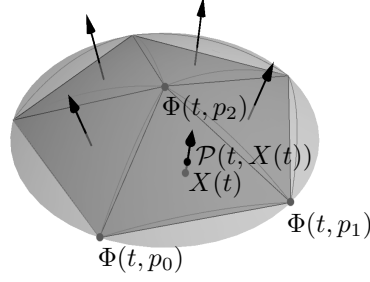


FIGURE 5.1. In a sketch we depict here a fan of evolving triangles, the transported vertices  $\Phi(t, p_0)$ ,  $\Phi(t, p_1)$ , and  $\Phi(t, p_2)$  of one specific moving triangle  $S^k(t)$ , and the projection  $\mathcal{P}(t, X(t))$  of a point  $X(t)$  in  $S^k(t)$  onto  $\Gamma(t)$ .

$\xi_2(x)p_2$  and  $\xi_0(x) + \xi_1(x) + \xi_2(x) = 1$ . Furthermore, let us now introduce the time continuous lift

$$\Psi^k(t, \cdot) : S^k \longrightarrow S^{l,k}(t), \quad x \longmapsto \Psi^k(t, x) = \Phi(t, \Phi^{-1}(t_k, \mathcal{P}^k(x))) \quad (5.3)$$

and the discrete surface evolution

$$\Upsilon^k(t, \cdot) : S^k \longrightarrow S^k(t), \quad x \longmapsto \sum_{i=0}^2 \xi_i(x) \Psi^k(t, p_i) \quad (5.4)$$

which will be used to go back and forth between evolving domains  $\Gamma(t)$  and the evolving discrete surface  $\Gamma_h(t)$ , where  $S^k(t)$  is the triangle generated via the motion of the vertices  $p$  of  $S^k$  along the trajectories  $\Phi(\cdot, p)$ , and  $\Gamma_h(t)$  the time continuous triangular surface consisting of these simplices.

Let us remark that  $\Upsilon^{k,k+1}(X_S^k)$  in condition (5.1) equals  $\Upsilon^k(t_{k+1}, X_S^k)$ . Figure

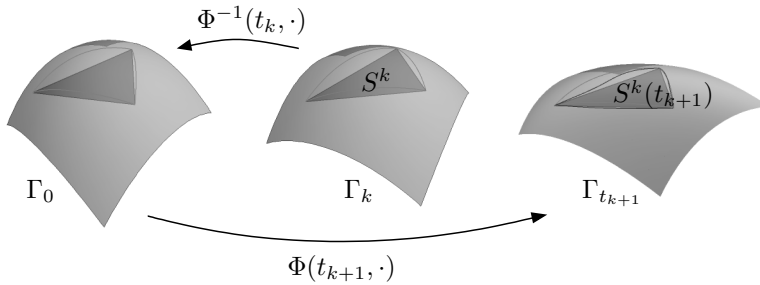


FIGURE 5.2. A single triangle and the nearby surface patch are shown in the initial configuration and at two consecutive time steps.

5.1 depicts a sketch of the involved geometric configuration. It is also important to notice here that the smoothness of these functions depends only on the regularity of  $\Phi(\cdot, \cdot)$ .

We now introduce an estimate for the distance between the continuous surface and the triangulation and for the ratio between cell areas and their lifted counterparts:

LEMMA 5.2. *Let  $d(t, x)$  be the signed distance from a point  $x$  to the surface  $\Gamma(t)$ , taking to be positive in the direction of the surface normal  $\nu$  and let  $m_S^{l,k}$  denote the measure of the lifted triangle  $S^{l,k}$ ,  $m_\sigma^{l,k}$  the measure of the lifted edge  $\sigma^{l,k}$ , then the estimates*

$$\sup_{0 \leq t \leq t_{max}} \|d(t, \cdot)\|_{L^\infty(\Gamma_h(t))} \leq Ch^2, \quad \sup_{k,S} \left| 1 - \frac{m_S^{l,k}}{m_S^k} \right| \leq Ch^2, \quad \sup_{k,\sigma} \left| 1 - \frac{m_\sigma^{l,k}}{m_\sigma^k} \right| \leq Ch^2$$

hold for a constant  $C$  depending only on the regularity assumptions.

PROOF: Notice that the function  $d(t, \cdot)$  is zero at vertices of the triangulation. Thus the piecewise affine Lagrangian interpolation of  $d(t, \cdot)$  vanishes and the first estimate immediately follows from standard interpolation estimates. Using the smoothness of  $d$  and the fact that, because of the regularity of the mesh, the normal direction on each triangle differs from the normals to the respective curved triangle only to the order  $h$ , we deduce from  $\nabla_{\Gamma(t)} d(t, \cdot) = 0$  on  $\Gamma(t)$  that  $\|\nabla_{S^k(t)} d(t, \cdot)\|_{L^\infty(\Gamma_h(t))} \leq Ch$ , where  $\nabla_{S^k(t)} d(t, \cdot)$  is the component of  $\nabla d(t, \cdot)$  tangential to  $S^k(t)$ . For the second estimate, we fix a triangle  $S^k$  and assume without any restriction that  $S^k \subset \{(\xi, 0) \mid \xi \in \mathbb{R}^2\}$ . Furthermore, we extend the projection  $\mathcal{P}^k$  onto a neighborhood of  $S^k$  in the following way:

$$\mathcal{P}_{ext}^k(\xi, \zeta) = (\xi, 0) + (\zeta - d(t_k, (\xi, 0))) \nabla d^T(t_k, (\xi, 0)).$$

Obviously,  $\mathcal{P}_{ext}^k = \mathcal{P}^k$  on  $S^k$ . From  $|d(t_k, (\xi, 0))| \leq Ch^2$  and  $|\nabla_{S^k} d(t_k, (\xi, 0))| \leq Ch$ , we deduce that

$$|\det(D\mathcal{P}_{ext}^k(\xi, 0)) - 1| \leq Ch^2,$$

where  $D\mathcal{P}_{ext}^k$  denotes the Jacobian of  $\mathcal{P}_{ext}^k$ . Hence, taking into account that the third column of the Jacobian  $\partial_\zeta \mathcal{P}_{ext}^k(\xi, 0) = \nabla d^T(t_k, (\xi, 0))$  has length 1 and is normal to  $\Gamma(t_k)$  at  $\mathcal{P}^k(\xi, 0)$ , we observe that  $|\det(D\mathcal{P}_{ext}^k(\xi, 0))|$  controls the transformation of area under the projection  $\mathcal{P}^k$  from  $S^k$  to  $S^{l,k}$ , which proves the claim.

The third estimate follows along the same line as the second estimate based on a straightforward adaptation of the argument.  $\square$

Next, we control the area defect between a transported lifted versus a lifted transported triangle:

LEMMA 5.3. *For each triangle  $S^k$  on  $\Gamma_h^k$  and all  $x$  in  $S^k$  the estimate*

$$|\mathcal{P}(t, \Upsilon^k(t, x)) - \Psi^k(t, x)| \leq C\tau h^2$$

holds for a constant  $C$  depending only the regularity assumptions. Furthermore, for the symmetric difference between  $S^{l,k}(t_{k+1})$  and  $S^{l,k+1}$  with  $A\Delta B := (A \setminus B) \cup (B \setminus A)$  one obtains

$$\mathcal{H}^{n-1}(S^{l,k}(t_{k+1})\Delta S^{l,k+1}) \leq C\tau h m_S^{k+1},$$

where  $\mathcal{H}^{n-1}$  is the  $(n-1)$ -dimensional Hausdorff measure of the considered continuous surface difference.

PROOF: At first, we notice that the function  $\Psi^k(t, \cdot)$  defined in (5.3) parametrizes the lifted and then transported triangle  $S^{l,k}(t)$  over  $S^k$  and  $\mathcal{P}(t, \Upsilon^k(t, \cdot))$  with  $\Upsilon^k(t, \cdot)$  defined in (5.4) parametrizes the transported and then lifted triangle  $\mathcal{P}(t, S^k(t))$  over  $S^k$ . These two functions share the same Lagrangian interpolation  $\Upsilon^k(t, \cdot)$  for any  $t$ , which implies the estimate

$$|\mathcal{P}(t, \Upsilon^k(t, x)) - \Psi^k(t, x)| \leq \beta(t)h^2$$

for every  $x \in S^k$ . Here,  $\beta(t)$  is a non negative and smooth function in time. From  $S^{l,k}(t_k) = S^{l,k}$  one deduces that  $\beta(\cdot)$  can be chosen such that  $\beta(t) \leq C|t - t_k|$  holds. Furthermore,  $C\tau h^2$  is also a bound for the maximum norm of the displacement function  $\mathcal{P}(t, \Upsilon^k(t, \cdot)) - \Psi^k(t, \cdot)$  on edges  $\sigma^k$ . Thus, taking into account that  $hm_\sigma^k \leq Cm_S^k$ , we obtain as a direct consequence the second claim.  $\square$

Based on this estimate, we immediately obtain the following corollary:

COROLLARY 5.4. *For any triangle  $S^k$  on  $\Gamma_h^k$  and any Lipschitz continuous function  $\omega(t, \cdot)$  defined on  $\Gamma(t)$  one obtains*

$$\left| \int_{S^{l,k}(t_{k+1})} \omega(t_{k+1}, x) da - \int_{S^{l,k+1}} \omega(t_{k+1}, x) da \right| \leq C\tau h m_S^{k+1}$$

for a constant  $C$  depending only on the regularity assumptions.

**5.2. Consistency estimates.** Next, with these geometric preliminaries at hand, we are able to derive a priori bounds for various consistency errors in conjunction with the finite volume approximation (3.6) of the continuous evolution (2.1).

LEMMA 5.5. *Let  $S^k$  be a triangle in  $\Gamma_h^k$  and  $t \in [t_k, t_{k+1}]$ , then for*

$$\begin{aligned} \mathcal{R}_1(S^{l,k}(t)) &:= \int_{S^{l,k}(t)} \nabla_{\Gamma(t)} \cdot (\mathcal{D}\nabla_{\Gamma(t)}u(t, \cdot)) da \\ &\quad - \int_{S^{l,k}(t_{k+1})} \nabla_{\Gamma(t_{k+1})} \cdot (\mathcal{D}\nabla_{\Gamma(t_{k+1})}u(t_{k+1}, \cdot)) da \end{aligned}$$

we obtain the estimate  $|\mathcal{R}_1(S^{l,k}(t))| \leq C\tau(1 + Ch^2)m_S^{k+1}$ .

PROOF: We recall that  $\nabla_{\Gamma(t)}u(t, x) = \nabla u^{ext}(t, x) - (\nabla u^{ext}(t, x) \cdot \nu(t, x))\nu(t, x)$  where  $u^{ext}(t, \cdot)$  is a constant extension of  $u(t, \cdot)$  in the normal direction  $\nu(t, \cdot)$  of  $\Gamma(t)$ . Any continuous and differentiable vector field  $v(t, \cdot)$  on  $\Gamma(t)$  can be extended in the same way for each component. Then, we obtain for the surface divergence of  $v(t, \cdot)$  at a point  $x$  on  $\Gamma(t)$  the representation  $\nabla_{\Gamma(t)} \cdot v(t, x) = \text{tr}((\text{Id} - \nu(t, x) \otimes \nu(t, x))\nabla v^{ext}(t, x))$ . Thus, we deduce from our regularity assumptions in Section 2 that the function  $(t, x) \mapsto \nabla_{\Gamma(t)} \cdot (\mathcal{D}\nabla_{\Gamma(t)}u(t, x))$  is Lipschitz in the time and space variable. This observations allows us to estimate  $|\mathcal{R}_1(S^{l,k}(t))|$  by  $C\tau m_S^{l,k+1}$ . Finally, taking into account Lemma 5.2 we obtain the postulated estimate.  $\square$

LEMMA 5.6. *For the edge  $\sigma^k$  between two adjacent triangles  $S^k$  and  $L^k$  the term*

$$\mathcal{R}_2(S^{l,k}|L^{l,k}) := \int_{\sigma^{l,k}} (\mathcal{D}\nabla_{\Gamma(t_k)}u(t_k, \cdot)) \cdot \mu_{\partial S^{l,k}} dl - \frac{m_\sigma^k \mathcal{M}_\sigma^k}{d_{S|L}^k} (u^{-l}(t_k, X_L^k) - u^{-l}(t_k, X_S^k)),$$

with  $\sigma^{l,k} = S^{l,k} \cap L^{l,k}$ , obeys the estimated  $|\mathcal{R}_2(S^{l,k}|L^{l,k})| \leq Cm_\sigma^k h$ .

PROOF: At first, we split the error term  $\mathcal{R}_2(S^{l,k}|L^{l,k})$  into corresponding consistency errors on the two adjacent triangles  $S^k$  and  $L^k$  taking into account the flux condition at the edge  $\sigma^{l,k}$ , the definition of  $\mathcal{M}_\sigma^k = \frac{\lambda_{S|\sigma}^k \lambda_{L|\sigma}^k d_{S|L}^k}{d_{L|\sigma}^k \lambda_{S|\sigma}^k + d_{S|\sigma}^k \lambda_{L|\sigma}^k}$  and the identity  $d_{S|L}^k = d_{S|\sigma}^k + d_{L|\sigma}^k$ . In fact, we obtain

$$\mathcal{R}_2(S^{l,k}|L^{l,k}) = \frac{m_\sigma^k \mathcal{M}_\sigma^k}{d_{S|L}^k} \left( \frac{d_{S|\sigma}^k}{m_\sigma^k \lambda_{S|\sigma}^k} \mathcal{R}_2(S^{l,k}|\sigma^{l,k}) - \frac{d_{L|\sigma}^k}{m_\sigma^k \lambda_{L|\sigma}^k} \mathcal{R}_2(L^{l,k}|\sigma^{l,k}) \right),$$

where

$$\mathcal{R}_2(S^{l,k}|\sigma^{l,k}) := \int_{\sigma^{l,k}} (\mathcal{D}\nabla_{\Gamma(t_k)} u(t_k, \cdot)) \cdot \mu_{\partial S^{l,k}} dl - m_\sigma^k \frac{u^{-l}(t_k, X_\sigma^k) - u^{-l}(t_k, X_S^k)}{d_{S|\sigma}^k} \lambda_{S|\sigma}^k. \quad (5.5)$$

Next, we estimate these error terms separately and obtain

$$\begin{aligned} \mathcal{R}_2(S^{l,k}|\sigma^{l,k}) = & \int_{\sigma^{l,k}} ((\mathcal{D}\nabla_{\Gamma(t_k)} u(t_k, \cdot)) \cdot \mu_{\partial S^{l,k}} - [(\mathcal{D}\nabla_{\Gamma(t_k)} u) \cdot \mu_{\partial S^{l,k}}](\mathcal{P}(t_k, X_\sigma^k))) dl \\ & + ([(\mathcal{D}\nabla_{\Gamma(t_k)} u) \cdot \mu_{\partial S^{l,k}}](\mathcal{P}(t_k, X_\sigma^k)) - [(\mathcal{D}\nabla_{\Gamma(t_k)} u^{-l}) \cdot \mu_{\partial S^{l,k}}](t_k, X_\sigma^k)) m_\sigma^{l,k} \\ & + [(\mathcal{D}\nabla_{\Gamma(t_k)} u^{-l}) \cdot \mu_{\partial S^{l,k}}](t_k, X_\sigma^k) (m_\sigma^{l,k} - m_\sigma^k) \\ & + \left( [(\mathcal{D}\nabla_{\Gamma(t_k)} u^{-l}) \cdot \mu_{\partial S^{l,k}}](t_k, X_\sigma^k) - [(\mathcal{D}\nabla_{\Gamma(t_k)} u^{-l}) \cdot \mu_{S|\sigma}^k](t_k, X_\sigma^k) \right) m_\sigma^k \\ & + \left( [(\mathcal{D}\nabla_{\Gamma(t_k)} u^{-l}) \cdot \mu_{S|\sigma}^k](t_k, X_\sigma^k) - [(\mathcal{D}\nabla_{S^k} u^{-l}) \cdot \mu_{S|\sigma}^k](t_k, X_\sigma^k) \right) m_\sigma^k \\ & + \left( \nabla_{S^k} u^{-l}(t_k, X_\sigma^k) \cdot (\mathcal{D}_{S|\sigma}^k \mu_{S|\sigma}^k) - \frac{u^{-l}(t_k, X_\sigma^k) - u^{-l}(t_k, X_S^k)}{d_{S|\sigma}^k} \|\mathcal{D}_{S|\sigma}^k \mu_{S|\sigma}^k\| \right) m_\sigma^k. \end{aligned}$$

Taking into account our regularity assumption from Section 2, Lemma 5.2, and the fact that  $\mathcal{D}_{S|\sigma}^k \mu_{S|\sigma}^k$  is imposed to be parallel to  $\overrightarrow{X_S^k X_\sigma^k}$  by (3.1) – indeed, even  $\frac{\mathcal{D}_{S|\sigma}^k \mu_{S|\sigma}^k}{\|\mathcal{D}_{S|\sigma}^k \mu_{S|\sigma}^k\|} = \frac{X_\sigma^k - X_S^k}{d_{S|\sigma}^k}$  – we finally observe that each term can be estimated from above by  $Cm_\sigma^k h$  for a constant  $C$  which only depends on the regularity assumptions. This proves the claim.  $\square$

The proof can be easily adapted to the case where the discrete diffusion tensor is defined on triangles as mentioned in section 3.

LEMMA 5.7. *For a cell  $S^k$  and the residual error term*

$$\begin{aligned} \mathcal{R}_3(S^{l,k}|S^{l,k+1}) = & \int_{S^{l,k}(t_{k+1})} u da - \int_{S^{l,k}(t_k)} u da \\ & - (m_S^{k+1} u^{-l}(t_{k+1}, X_S^{k+1}) - m_S^k u^{-l}(t_k, X_S^k)) \end{aligned}$$

one obtains the estimate  $|\mathcal{R}_3(S^{l,k}|S^{l,k+1})| \leq C\tau h m_S^{k+1}$ .

PROOF: At first, let us recall that  $\Psi^k(t, \cdot)$ ,  $\Upsilon^k(t, \cdot)$ , and  $\mathcal{P}(t_{k+1}, \Upsilon^k(t_{k+1}, \cdot))$  parametrize  $S^{l,k}(t)$ ,  $S^k(t)$ , and  $S^{l,k+1}$  over the triangle  $S^k$ . Via standard quadrature error estimates and due to the regularity assumptions on  $\Phi$  and  $u$  given in Section 2, we obtain for the smooth quadrature error function

$$Q(t) := \int_{S^{l,k}(t)} u(t, x) \, da - u(t, \mathcal{P}(t, \Upsilon^k(t, X_S^k))) \mathcal{H}^{n-1}(S^{l,k}(t))$$

the estimate  $|Q(t) - Q(t_k)| \leq \tilde{\beta}(t) h \mathcal{H}^{n-1}(S^{l,k}(t))$ , where  $\tilde{\beta}$  is a smooth, non negative function in time. From  $Q(t_k) - Q(t_k) = 0$  we deduce that  $\tilde{\beta}(t) \leq C|t - t_k|$  (cf. also the proof of Lemma 5.3). Based on an analogous argument we obtain for the continuity modulus of  $\tilde{Q}(t) := \int_{\mathcal{P}(t, S^k(t))} da - \int_{S^k(t)} da$  that

$$\tilde{Q}(t_{k+1}) - \tilde{Q}(t_k) \leq C\tau h^2 m_S^k.$$

Making use of our notation we observe that the left hand side equals  $(m_S^{l,k+1} - m_S^{k+1}) - (m_S^{l,k} - m_S^k)$ . We now split the residual into

$$\begin{aligned} \mathcal{R}_3(S^{l,k}|S^{l,k+1}) &= Q(t_{k+1}) - Q(t_k) \\ &\quad + u(t_{k+1}, \mathcal{P}(t_{k+1}, \Upsilon^k(t_{k+1}, X_S^k))) \left( \mathcal{H}^{n-1}(S^{l,k}(t_{k+1})) - m_S^{l,k+1} \right) \\ &\quad + \left( u(t_{k+1}, \mathcal{P}(t_{k+1}, \Upsilon^k(t_{k+1}, X_S^k))) - u^{-l}(t_{k+1}, X_S^{k+1}) \right) m_S^{l,k+1} \\ &\quad + u^{-l}(t_{k+1}, X_S^{k+1}) \left[ \left( m_S^{l,k+1} - m_S^{k+1} \right) - \left( m_S^{l,k} - m_S^k \right) \right] \\ &\quad + \left( u^{-l}(t_{k+1}, X_S^{k+1}) - u^{-l}(t_{k+1}, \Upsilon^k(t_{k+1}, X_S^k)) \right) \left( m_S^{l,k} - m_S^k \right) \\ &\quad + \left( u^{-l}(t_{k+1}, \Upsilon^k(t_{k+1}, X_S^k)) - u^{-l}(t_k, X_S^k) \right) \left( m_S^{l,k} - m_S^k \right). \end{aligned}$$

Finally, applying the above estimates, (5.1), Lemma 5.2, and Lemma 5.3, we get

$$\begin{aligned} |\mathcal{R}_3(S^{l,k}|S^{l,k+1})| &\leq C(\tau h^2 m_S^{k+1} + \tau h m_S^k + \tau h m_S^{k+1} + \tau h^2 m_S^{k+1} + \tau h^3 m_S^k + \tau h^2 m_S^k) \\ &\leq C\tau h m_S^{k+1}. \end{aligned}$$

□

LEMMA 5.8. *For a cell  $S^k$  and the residual error term*

$$\mathcal{R}_4(S^{l,k}|S^{l,k+1}) = \int_{t_k}^{t_{k+1}} \int_{S^{l,k}(t)} g \, da \, dt - \tau m_S^{k+1} g^{-l}(t_{k+1}, X_S^{k+1})$$

one achieves the estimate  $|\mathcal{R}_4(S^{l,k}|S^{l,k+1})| \leq C\tau(\tau + h)m_S^{k+1}$ .

PROOF: We expand the residual by

$$\begin{aligned}
\mathcal{R}_4(S^{l,k}|S^{l,k+1}) &= \int_{t_k}^{t_{k+1}} \left( \int_{S^{l,k}(t)} g(t,x) \, da - \int_{S^{l,k}(t_{k+1})} g(t_{k+1},x) \, da \right) dt \\
&\quad + \tau \left( \int_{S^{l,k}(t_{k+1})} g(t_{k+1},x) \, da - \int_{S^{l,k+1}} g(t_{k+1},x) \, da \right) \\
&\quad + \tau \left( \int_{S^{l,k+1}} g(t_{k+1},x) \, da - g^{-l}(t_{k+1}, X_S^{k+1}) m_S^{l,k+1} \right) \\
&\quad + \tau \left( m_S^{l,k+1} - m_S^{k+1} \right) g^{-l}(t_{k+1}, X_S^{k+1}).
\end{aligned}$$

Now we use a standard quadrature estimate, Lemma 5.2, Lemma 5.3, and Corollary 5.4, which yields

$$\begin{aligned}
|\mathcal{R}_4(S^{l,k}|S^{l,k+1})| &\leq C(\tau^2 \mathcal{H}^{n-1}(S^{l,k}(t_{k+1})) + \tau^2 h m_S^{k+1} + \tau h m_S^{k+1} + \tau h^2 m_S^{k+1}) \\
&\leq C\tau(\tau + h)m_S^{k+1}.
\end{aligned}$$

□

**5.3. Proof of Theorem 5.1.** As in Section 2 (cf. (3.2), (3.3), and (3.4)) let us consider the following triangle wise flux formulation of the continuous problem (2.1):

$$\int_{S^{l,k}(t_{k+1})} u \, da - \int_{S^{l,k}(t_k)} u \, da - \int_{t_k}^{t_{k+1}} \int_{\partial S^{l,k}(t)} \mathcal{D}\nabla_{\Gamma} u \cdot \mu_{\partial S^{l,k}(t)} \, dl \, dt = \int_{t_k}^{t_{k+1}} \int_{S^{l,k}(t)} g \, da \, dt$$

From this equation we subtract the discrete counterpart (3.6)

$$m_S^{k+1} U_S^{k+1} - m_S^k U_S^k - \tau \sum_{\sigma \subset \partial S} m_{\sigma}^{k+1} \mathcal{M}_{\sigma}^{k+1} \frac{U_L^{k+1} - U_S^{k+1}}{d_{S|L}^{k+1}} = \tau m_S^{k+1} G_S^{k+1}$$

and multiply this with  $E_S^{k+1} = u^{-l}(t_{k+1}, X_S^{k+1}) - U_S^{k+1}$ . Hence, we obtain

$$\begin{aligned}
&\mathcal{R}_3(S^{l,k}|S^{l,k+1}) E_S^{k+1} + m_S^{k+1} (E_S^{k+1})^2 - m_S^k E_S^{k+1} E_S^k \\
&\quad - \left( \int_{t_k}^{t_{k+1}} \mathcal{R}_1(S^{l,k}(t)) \, dt \right) E_S^{k+1} - \tau \sum_{\sigma \subset \partial S} \mathcal{R}_2(S^{l,k+1}|L^{l,k+1}) E_S^{k+1} \\
&\quad - \tau \sum_{\sigma \subset \partial S} \frac{m_{\sigma}^{k+1} \mathcal{M}_{\sigma}^{k+1}}{d_{S|L}^{k+1}} (E_L^{k+1} - E_S^{k+1}) E_S^{k+1} = \mathcal{R}_4(S^{l,k}|S^{l,k+1}) E_S^{k+1}.
\end{aligned}$$

Now, we sum over all simplices and obtain

$$\begin{aligned}
&\sum_S m_S^{k+1} (E_S^{k+1})^2 + \tau \sum_{\sigma=S \cap L} \frac{m_{\sigma}^{k+1} \mathcal{M}_{\sigma}^{k+1}}{d_{S|L}^{k+1}} (E_L^{k+1} - E_S^{k+1})^2 = \sum_S m_S^k E_S^{k+1} E_S^k \\
&\quad - \sum_S \left( \mathcal{R}_3(S^{l,k}|S^{l,k+1}) - \int_{t_k}^{t_{k+1}} \mathcal{R}_1(S^{l,k}(t)) \, dt - \mathcal{R}_4(S^{l,k}|S^{l,k+1}) \right) E_S^{k+1} \\
&\quad + \tau \sum_S \sum_{\sigma \subset \partial S} \mathcal{R}_2(S^{l,k+1}|L^{l,k+1}) E_S^{k+1}.
\end{aligned}$$



Observing that  $\mathcal{R}_2(S^{l,k+1}|L^{l,k+1}) = -\mathcal{R}_2(L^{l,k+1}|S^{l,k+1})$  the last term on the right hand side can be rewritten and estimated as follows

$$\begin{aligned} & \sum_{\sigma=S \cap L} \mathcal{R}_2(S^{l,k+1}|L^{l,k+1}) \sqrt{\frac{d_{S|L}^{k+1}}{m_\sigma^{k+1} \mathcal{M}_\sigma^{k+1}}} \frac{\sqrt{m_\sigma^{k+1} \mathcal{M}_\sigma^{k+1}} (E_L^{k+1} - E_S^{k+1})}{\sqrt{d_{S|L}^{k+1}}} \\ & \leq \left( \sum_{\sigma=S \cap L} \mathcal{R}_2(S^{l,k+1}|L^{l,k+1})^2 \frac{d_{S|L}^{k+1}}{m_\sigma^{k+1} \mathcal{M}_\sigma^{k+1}} \right)^{\frac{1}{2}} \|E^{k+1}\|_{1, \Gamma_h^{k+1}} \\ & \leq C \left( \sum_S m_S^{k+1} h^2 \right)^{\frac{1}{2}} \|E^{k+1}\|_{1, \Gamma_h^{k+1}} \leq C h \mathcal{H}^{n-1}(\Gamma_h^{k+1})^{\frac{1}{2}} \|E^{k+1}\|_{1, \Gamma_h^{k+1}}. \end{aligned}$$

Here, we have used Lemma 5.6 and the estimate  $m_\sigma^{k+1} h \leq C m_S^{k+1}$  for  $\sigma \subset \partial S$ . Now, we take into account the consistency results from Corollary 5.4, Lemma 5.5, Lemma 5.7, Lemma 5.8, apply Young's and Cauchy's inequality and achieve the estimate

$$\begin{aligned} & \|E^{k+1}\|_{L^2(\Gamma_h^{k+1})}^2 + \tau \|E^{k+1}\|_{1, \Gamma_h^{k+1}}^2 \\ & \leq \frac{1}{2} \|E^{k+1}\|_{L^2(\Gamma_h^{k+1})}^2 + \frac{1}{2} \|E^k\|_{L^2(\Gamma_h^k)}^2 + \frac{1}{2} \max_k \max_S \left| 1 - \frac{m_S^k}{m_S^{k+1}} \right| \|E^k\|_{L^2(\Gamma_h^k)}^2 \\ & \quad + C(\tau h + \tau^2(1 + C h^2) + \tau(\tau + h)) \mathcal{H}^{n-1}(\Gamma_h^{k+1})^{\frac{1}{2}} \|E^{k+1}\|_{L^2(\Gamma_h^{k+1})} \\ & \quad + C \tau h \mathcal{H}^{n-1}(\Gamma_h^{k+1})^{\frac{1}{2}} \|E^{k+1}\|_{1, \Gamma_h^{k+1}}. \end{aligned}$$

Based on our assumption that the triangulation is advected in time we can estimate  $\left| 1 - \frac{m_S^k}{m_S^{k+1}} \right| \leq C \tau$ . Again applying Young's inequality to the last two term on the right hand side we get

$$\begin{aligned} & C(\tau h + \tau^2(1 + C h^2) + \tau(\tau + h)) \mathcal{H}^{n-1}(\Gamma_h^{k+1})^{\frac{1}{2}} \frac{1}{2} \|E^{k+1}\|_{L^2(\Gamma_h^{k+1})} \\ & \leq C \tau \|E^{k+1}\|_{L^2(\Gamma_h^{k+1})}^2 + C \tau(\tau + h)^2 \mathcal{H}^{n-1}(\Gamma_h^{k+1}), \\ & C \tau h \mathcal{H}^{n-1}(\Gamma_h^{k+1})^{\frac{1}{2}} \|E^{k+1}\|_{1, \Gamma_h^{k+1}} \leq \frac{\tau}{2} \|E^{k+1}\|_{1, \Gamma_h^{k+1}}^2 + \frac{\tau C^2 h^2}{2} \mathcal{H}^{n-1}(\Gamma_h^{k+1}). \end{aligned}$$

Hence, taking into account that  $\mathcal{H}^{n-1}(\Gamma_h^{k+1})$  is uniformly bounded we obtain the estimate

$$(1 - C\tau) \|E^{k+1}\|_{L^2(\Gamma_h^{k+1})}^2 + \frac{\tau}{2} \|E^{k+1}\|_{1, \Gamma_h^{k+1}}^2 \leq (1 + C\tau) \|E^k\|_{L^2(\Gamma_h^k)}^2 + C\tau(\tau + h)^2. \quad (5.6)$$

At first, we skip the second term on the left hand side, use the inequality  $\frac{(1+C\tau)}{(1-C\tau)} \leq (1+c\tau)$  for sufficiently small time step  $\tau$  and a constant  $c > 0$ , and obtain via iteration (cf. also the proof of Theorem 4.1):

$$\begin{aligned} \|E^{k+1}\|_{L^2(\Gamma_h^{k+1})}^2 & \leq (1 + c\tau) \|E^k\|_{L^2(\Gamma_h^k)}^2 + C\tau(\tau + h)^2 \\ & \leq \dots \leq (1 + c\tau)^{k+1} \|E^0\|_{L^2(\Gamma_h^0)}^2 + \sum_{i=1}^k \tau(1 + c\tau)^{i-1} (\tau + h)^2 \\ & \leq e^{c t_k} \left( \|E^0\|_{L^2(\Gamma_h^0)}^2 + t_k (\tau + h)^2 \right) \end{aligned}$$

This implies the first claim of the theorem:

$$\max_{k=1, \dots, k_{max}} \|E^k\|_{L^2(\Gamma_h^k)}^2 \leq C(\tau + h)^2$$

Finally, taking into account this estimate and summing over  $k = 0, \dots, k_{max} - 1$  in (5.6) we obtain also the claimed estimate for the discrete  $H^1$ -norm of the error:

$$\sum_{k=1, \dots, k_{max}} \tau \|E^k\|_{1, \Gamma_h^k}^2 \leq C(\tau + h)^2$$

□

**6. Coupled reaction diffusion and advection model.** In what follows we will generalize our finite volume approach by considering a source term  $g$  which depends on the solution and an additional tangential advection term  $\nabla_\Gamma \cdot (wu)$ . Here,  $w$  is an additional tangential transport velocity on the surface, which transports the density  $u$  along the moving interface  $\Gamma$  instead of just passively advecting it with interface. We assume the mapping  $(t, x) \rightarrow w(t, \Phi(t, x))$  to be in  $C^1([0, t_{max}], C^1(\Gamma_0))$ . Furthermore, we suppose  $g$  to be Lipschitz continuous. An extension to a reaction term which also explicitly depends on time and position is straightforward. Hence, we investigate the evolution problem

$$\dot{u} + u \nabla_\Gamma \cdot v - \nabla_\Gamma \cdot (\mathcal{D} \nabla_\Gamma u) + \nabla_\Gamma \cdot (wu) = g(u) \quad \text{on } \Gamma = \Gamma(t). \quad (6.1)$$

In what follows, let us consider an appropriate discretization for both terms. For the reaction term, we consider the time explicit approximation

$$\int_{t_k}^{t_{k+1}} \int_{S^{l,k}(t)} g(u(t, x)) \, da \, dt \approx \tau m_S^k g(u(t_k, \mathcal{P}^k X_S^k)) \quad (6.2)$$

and then replace  $u(t_k, \mathcal{P}^k(X_S^k))$  by  $U_S^k$  in the actual numerical scheme. Furthermore, we take into account an upwind discretization of the additional transport term to ensure robustness also in a regime where the transport induced by  $w$  dominates the diffusion. Here, we confine to a classical first order upwind discretization. Thus, on each edge  $\sigma^k = S^k \cap L^k$  of a triangle  $S^k$  facing to the adjacent triangle  $L^k$  we define an averaged outward pointing co-normal  $\mu_{S|L}^k = |\mu_{\partial S} - \mu_{\partial L}|^{-1}(\mu_{\partial S} - \mu_{\partial L})$ . In particular  $\mu_{S|L}^k = -\mu_{L|S}^k$  holds. If  $\mu_{S|L}^k \cdot w^{-l}(t_k, X_\sigma^k) \geq 0$  the upwind direction is pointing inward and we define  $u^+(t_k, X_\sigma^k) := u^{-l}(t_k, X_S^k)$ , otherwise  $u^+(t_k, X_\sigma^k) := u^{-l}(t_k, X_L^k)$ . Once, the upwind direction is identified, we take into account the classical approach by Enquist and Osher [12] and obtain the approximation:

$$\int_{t_k}^{t_{k+1}} \int_{S^{l,k}(t)} \nabla_\Gamma \cdot (wu) \, da \, dt \approx \tau \sum_{\sigma \subset \partial S} m_\sigma^k (\mu_{\sigma,S}^k \cdot w^{-l}(t_k, X_\sigma^k)) u^+(t_k, X_\sigma^k) \quad (6.3)$$

Finally, we again replace  $u^{-l}(t_k, X_S^k)$  by the discrete nodal values  $U_S^k$  and denote these by  $U_\sigma^{k,+}$ . For the sake of completeness let us resume the resulting scheme:

$$\begin{aligned} m_S^{k+1} U_S^{k+1} - m_S^k U_S^k &= \tau \sum_{\sigma \subset \partial S} m_\sigma^{k+1} \mathcal{M}_\sigma^{k+1} \frac{U_L^{k+1} - U_S^{k+1}}{d_{S|L}^{k+1}} \\ &\quad + \tau m_S^k g(U_S^k) - \tau \sum_{\sigma \subset \partial S} m_\sigma^k (\mu_{S|L}^k \cdot w^{-l}(t_k, X_\sigma^k)) U_\sigma^{k,+} \end{aligned} \quad (6.4)$$

Obviously, due to the fully explicit discretization of the additional terms Proposition 3.2 still applies and guarantees existence and uniqueness of a discrete solution. Furthermore, the convergence result can be adapted and the error estimate postulated in Theorem 5.1 holds. To see this, let us first consider the nonlinear source term  $g(u)$  and estimate

$$\begin{aligned}
& \int_{t_k}^{t_{k+1}} \int_{S^{l,k}(t)} g(u(t, x)) \, da \, dt - \tau m_S^k g(U_S^k) \\
& \leq \int_{t_k}^{t_{k+1}} \left( \int_{S^{l,k}(t)} g(u(t, x)) \, da - \int_{S^{l,k}} g(u(t_k, x)) \, da \right) dt \\
& \quad + \tau \left( \int_{S^{l,k}} g(u(t_k, x)) \, da - m_S^{l,k} g(u^{-l}(t_k, X_S^k)) \right) dt + \tau (m_S^{l,k} - m_S^k) g(u^{-l}(t_k, X_S^k)) \\
& \quad + \tau m_S^k (g(u^{-l}(t_k, X_S^k)) - g(U_S^k)) \\
& \leq C (\tau^2 \mathcal{H}^{n-1}(S^{l,k}) + \tau h m_S^k + \tau h^2 m_S^k + C_{Lip}(g) \tau m_S^k E_S^k) ,
\end{aligned}$$

where  $C_{Lip}(g)$  denotes the Lipschitz constant of  $g$ . In the proof of Theorem 5.1 we already have treated terms identical to the first three on the right hand side. For the last term we obtain after multiplication with the nodal error  $E_S^{k+1}$  and a summation over all cells  $S$

$$\begin{aligned}
C_{Lip}(g) \tau \sum_S m_S^k E_S^k E_S^{k+1} & \leq C_{Lip}(g) \tau \max_S \left( \frac{m_S^k}{m_S^{k+1}} \right)^{\frac{1}{2}} \|E^k\|_{L^2(\Gamma_h(t_k))} \|E^{k+1}\|_{L^2(\Gamma_h(t_k))} \\
& \leq C \tau \left( \|E^k\|_{L^2(\Gamma_h(t_k))}^2 + \|E^{k+1}\|_{L^2(\Gamma_h(t_{k+1}))}^2 \right) .
\end{aligned}$$

Taking into account these additional error terms the estimate (5.6) remains unaltered. Next, we investigate the error due to the additional advection term and rewrite

$$\begin{aligned}
& \int_{t_k}^{t_{k+1}} \int_{S^{l,k}(t)} \nabla_{\Gamma} \cdot (wu) \, da \, dt - \tau \sum_{\sigma \subset \partial S} m_{\sigma}^k (\mu_{\sigma,S}^k \cdot w^{-l}(t_k, X_{\sigma}^k)) U_{\sigma}^{k,+} \\
& = \int_{t_k}^{t_{k+1}} \int_{S^{l,k}(t)} \nabla_{\Gamma} \cdot (wu) \, da \, dt - \tau \int_{S^{l,k}} \nabla_{\Gamma} \cdot (wu) \, da \\
& \quad + \sum_{\substack{\sigma \subset \partial S \\ \sigma = S \cap L}} (\tau \mathcal{R}_5(S^{l,k}|L^{l,k}) + \tau \mathcal{F}(S^{l,k}|L^{l,k}) E_{\sigma}^{k,+}) ,
\end{aligned}$$

where  $\mathcal{R}_5(S^{l,k}|L^{l,k}) = \int_{\sigma^{l,k}} \mu_{\partial S^{l,k}} \cdot w u \, dl - m_{\sigma}^k w^{-l}(t_k, X_{\sigma}^k) \cdot \mu_{S|L}^k u^+(t_k, X_{\sigma}^k)$  is an edge residual,  $\mathcal{F}(S^{l,k}|L^{l,k}) = m_{\sigma}^k w^l(t_k, X_{\sigma}^k) \cdot \mu_{S|L}^k$  a flux term on the edge  $\sigma^{l,k} = S^{l,k} \cap L^{l,k}$ , and  $E_{\sigma}^{k,+} = u^+(t_k, X_{\sigma}^k) - U_{\sigma}^{k,+}$  a piecewise constant upwind error function on the discrete surface  $\Gamma_h^k$ . The first term in the above error representation can again be estimated by  $C \tau^2 \mathcal{H}^{n-1}(S^{l,k})$ . From  $|u^+(t_k, X_{\sigma}^k) - u^{-l}(t_k, X_{\sigma}^k)| \leq Ch$ , we deduce by similar arguments as in the proof of Lemma 5.6 that  $|\mathcal{R}_5(S^{l,k}|L^{l,k})| \leq Ch m_{\sigma}^k$ . Furthermore, the antisymmetry relations  $\mathcal{R}_5(S^{l,k}|L^{l,k}) = -\mathcal{R}_5(L^{l,k}|S^{l,k})$  and  $\mathcal{F}(S^{l,k}|L^{l,k}) = -\mathcal{F}(L^{l,k}|S^{l,k})$  hold (cf. the same relation for  $\mathcal{R}_2(S^{l,k}|L^{l,k})$ ).

After multiplication with the nodal error  $E_S^{k+1}$  and summation over all cells  $S$  we obtain

$$\begin{aligned}
& \tau \sum_S \sum_{\substack{\sigma \subset \partial S \\ \sigma = S \cap L}} (\mathcal{R}_5(S^{l,k}|L^{l,k}) + \tau \mathcal{F}(S^{l,k}|L^{l,k}) E_\sigma^{k,+}) E_S^{k+1} \\
& \leq \tau \sum_{\sigma = S \cap L} (\mathcal{R}_5(S^{l,k}|L^{l,k}) (E_S^{k+1} - E_L^{k+1}) + \mathcal{F}(S^{l,k}|L^{l,k}) E_\sigma^{k,+} (E_S^{k+1} - E_L^{k+1})) \\
& \leq \tau \left( \sum_{\sigma = S \cap L} (\mathcal{R}_5(S^{l,k}|L^{l,k}) + \mathcal{F}(S^{l,k}|L^{l,k}) E_\sigma^{k,+})^2 \frac{d_{S|L}^{k+1}}{m_\sigma^{k+1} \mathcal{M}_\sigma^{k+1}} \right)^{\frac{1}{2}} \|E^{k+1}\|_{1, \Gamma_h^{k+1}} \\
& \leq C \tau (h \mathcal{H}^{n-1}(\Gamma_h^k)^{\frac{1}{2}} + \left( \sum_{\sigma = S \cap L} m_S^k (E_\sigma^{k,+})^2 \right)^{\frac{1}{2}}) \|E^{k+1}\|_{1, \Gamma_h^{k+1}} \\
& \leq \frac{\tau}{4} \|E^{k+1}\|_{1, \Gamma_h^{k+1}}^2 + C \tau h^2 + C \tau \|E^k\|_{L^2(\Gamma_h^k)}^2.
\end{aligned}$$

Here, we have applied the straightforward estimate  $\|E^{k,+}\|_{L^2(\Gamma_h^k)} \leq C \|E^k\|_{L^2(\Gamma_h^k)}$  and Young's inequality. Again, taking into account these error terms due to the added advection in the original error estimate (5.6) solely the constant in front of the term  $\|E^{k+1}\|_{1, \Gamma_h^{k+1}}^2$  on the left hand side of (5.6) is slightly reduced.

Thus, both the explicit discretization of a nonlinear reaction term and the upwind discretization of the additional tangential advection still allow us to establish the error estimate postulated in Theorem 5.1.

**7. Numerical results.** To numerically simulate the evolution problem (2.1) we first have to set up a family of triangular meshes, which are consistent with the assumption made above. We generate these meshes based on an implicit description of the underlying initial surface and apply an adaptive polygonization method proposed by de Araújo and Pires in [6, 5]. This method polygonizes implicit surfaces along an evolving front with triangles whose sizes are adapted to the local radius of curvature. Afterwards, using a technique similar to the one developed by Persson in [19] we modify triangles to ensure the orthogonality condition (3.1). We refer also to [9] for a computational approach to anisotropic centroidal Voronoi meshes. Already in Figures 3.1 and 3.3 we have depicted a corresponding family of meshes.

As a first example, we consider a family of expanding and collapsing spheres with radius  $r(t) = 1 + \sin^2(\pi t)$ , and a function  $u(t, \theta, \lambda) = \frac{1}{r^2(t)} \exp\left(-6 \int_0^t \frac{1}{r^2(\tau)} d\tau\right) \cdot \sin(2\theta) \cos(\lambda)$  where  $\theta$  is the inclination and  $\lambda$  the azimuth. The function  $u$  solves (2.1) on this family of spheres for  $\mathcal{D} = \text{Id}$  and  $g = 0$ . We compute the numerical solution on successively refined surface triangulations on the time interval  $[0, 1]$ . Table 7.1 presents the different grids and the errors in the discrete  $L^\infty(L^2)$  norm and discrete energy semi norm (3.8), respectively. Indeed, the observed error decay is consistent with the convergence result in Theorem 5.1.

Next, we consider on the same geometry the advection vector  $\omega(t, x) = (0, 0, 30) - (\nu(t, x) \cdot (0, 0, 30)) \nu(t, x)$  with  $\nu(t, x)$  being the normal to the surface  $\Gamma(t)$ , and the source term  $g(t, \theta, \lambda) = 2c(t) (-\sin(2\theta) \cos(\lambda) (\omega(t, x) \cdot \nu(t, x)) + \cos(2\theta) \cos(\lambda) (\omega \cdot e_\theta) - \cos(\theta) \sin(\lambda) (\omega \cdot e_\lambda))$  where  $e_\theta = (\cos(\theta) \cos(\lambda), \cos(\theta) \sin(\lambda), -\sin(\theta))$ ,  $e_\lambda = (-\sin(\lambda), \cos(\lambda), 0)$  and  $c(t) = \frac{1}{r^3(t)} \exp\left(-6 \int_0^t \frac{1}{r^2(\tau)} d\tau\right)$ . The function  $u(t, \theta, \lambda) = \frac{1}{r^2(t)} \exp\left(-6 \int_0^t \frac{1}{r^2(\tau)} d\tau\right) \cdot \sin(2\theta) \cos(\lambda)$  now solves 6.1. In fact  $\omega$  has been chosen to be at the limit of the CFL-condition on the finest grid, characterizing the strength

of the advection. Table 7.2 presents the errors in the discrete  $L^\infty(L^2)$  norm and discrete energy semi norm (3.8), using the same triangulations as above. The observed error decay is again consistent with the convergence result in Theorem 5.1.

In fact, even though the solution – and thus its interpolation properties – are identical to the previous example, we see a reduced order of convergence due to the transport part of the equation. In general we could improve the order of convergence by using a higher order slope limiting and replacing condition (5.1) by

$$|\Upsilon^{k,k+1}(X_S^k) - X_S^{k+1}| \leq Ch^2\tau.$$

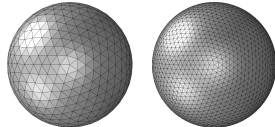
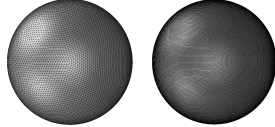
		$h(0)$ $\max_{t \in [0,1]} h(t)$		norm of the error	
				$L^\infty(L^2)$	$L^\infty(H^1)$
	0.2129	0.4257	$32.941 \cdot 10^{-4}$	$22.999 \cdot 10^{-3}$	
	0.1069	0.2138	$8.036 \cdot 10^{-4}$	$8.348 \cdot 10^{-3}$	
	0.0535	0.1070	$1.764 \cdot 10^{-4}$	$2.950 \cdot 10^{-3}$	
	0.0268	0.0536	$0.423 \cdot 10^{-4}$	$1.047 \cdot 10^{-3}$	

TABLE 7.1

On the left, the different triangulations used for the convergence test are depicted. The table on the right displays the numerical error on these grids in two different norms, when compared to the explicit solution. The time discretization was chosen as  $\tau = 1/32000 \ll h^2$  in all four computations.

$h(0)$ $\max_{t \in [0,1]} h(t)$		norm of the error	
		$L^\infty(L^2)$	$L^\infty(H^1)$
0.2129	0.4257	$25.53 \cdot 10^{-2}$	$11.615 \cdot 10^{-1}$
0.1069	0.2138	$14.26 \cdot 10^{-2}$	$7.089 \cdot 10^{-1}$
0.0535	0.1070	$7.61 \cdot 10^{-2}$	$3.985 \cdot 10^{-1}$
0.0268	0.0536	$3.95 \cdot 10^{-2}$	$2.125 \cdot 10^{-1}$

TABLE 7.2

The table displays the numerical error when compared to the explicit solution, in the advection dominated setting on the same grids as in Table 7.1. The time discretization was chosen as  $\tau = 1/32000 \ll h^2$  in all four computations.

Figure 7.1 shows the finite volume solution for the heat equation without source term. In the first row the sphere expands with constant velocity in normal direction, and the initial data has local support, while in the second row the sphere expands into an ellipsoid and the initial data is constant. Furthermore, we have computed isotropic and anisotropic diffusion on a rotating torus with zero initial data and time constant or time periodic source term, respectively. Figures 7.2 and 7.3 demonstrate

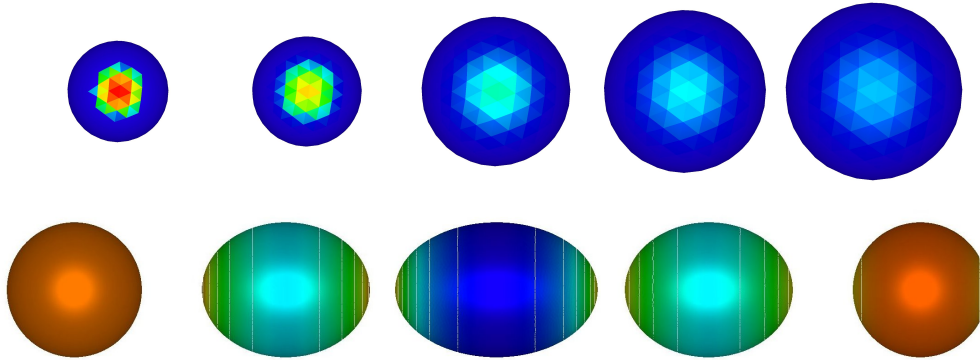


FIGURE 7.1. In the top row the heat equation ( $\mathcal{D} = \text{Id}$ ) is solved on an expanding sphere for initial data with local support on a relatively coarse evolving grid consisting of 956 triangles. The density is color coded from blue to red at different time steps. In the bottom row, an anisotropic expansion and later reverse contraction of a sphere with constant initial data computed on an evolving surface is depicted. Here a significantly finer discretization consisting of 18462 triangles is taken into account. Again we plot the density at different time steps. One clearly observes an inhomogeneous density with maxima on the less stretched poles during the expansion phase followed by an advective concentration of density close to the symmetry plane during the contraction phase.

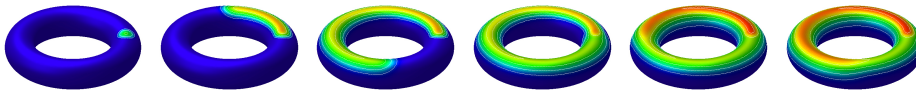


FIGURE 7.2. The solution of the isotropic heat equation is computed on a torus with smaller radius 1 and larger radius 4. The torus is triangulated with 21852 triangles and 10926 points, and it rotates around its center twice during the evolution process. As initial data we consider  $u_0 = 0$  and take into account a source term  $g$  with local support inside a geodesic ball of radius 0.5. The source term is considered to be time independent. The surface velocity implies a transport which together with the source term and the isotropic diffusion leads to the observed trace type solution pattern.

the different joint effects of transport and isotropic diffusion, similar to Figure 2 and 3 in [11]. In Figure 7.4 we consider the same problem as in Figure 7.3 except that

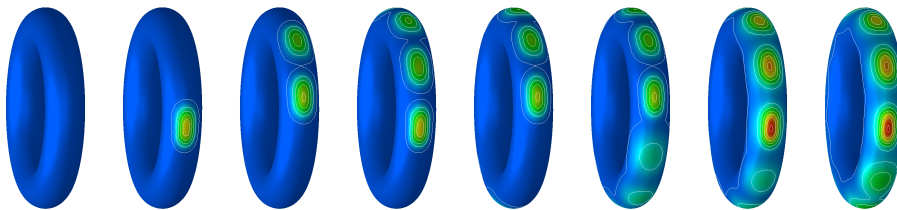


FIGURE 7.3. A similar computation as in Figure 7.2 has been performed, but with a pulsating source  $g$  with a 10 pulses during a complete rotation of the torus. The source is located at a slightly different position, and in order to pronounce the effect of the dynamics, the color scale is logarithmic.

this time the underlying diffusion tensor is anisotropic, i. e. we have chosen the

tensor

$$\mathcal{D} = \begin{pmatrix} \frac{1}{25} & 0 & 0 \\ 0 & 1 & 0 \\ 0 & 0 & 1 \end{pmatrix}$$

in  $\mathbb{R}^{3,3}$  whose restriction on the tangent bundle is considered as the diffusion in (2.1). The underlying grids have already been rendered in Figure 3.3. Finally, we combine

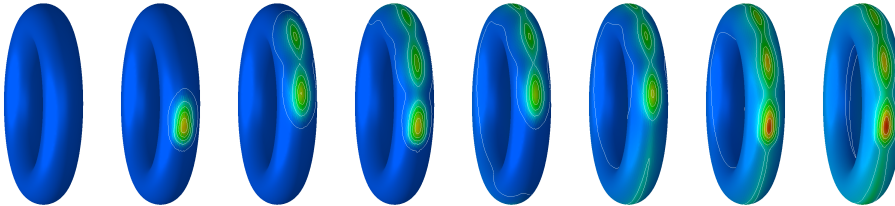


FIGURE 7.4. As in Figure 7.3 diffusion on a rotating torus with a pulsating sources is investigated. This time the diffusion is anisotropic with a smaller diffusion coefficient in the direction perpendicular to the torus' center plane. Again the color scale is logarithmic. The different diffusion lengths in the different directions can be clearly observed in the shape and distance of the isolines at later times and further away from the source.

the diffusion process on evolving surfaces with an additional (gravity type) advection term. As evolving geometry we have selected one with an initial four-fold symmetry undergoing a transition to the sphere (cf. Figure 3.1 for an corresponding triangular mesh, which is further refined for the actual computation). The advection direction is the projection of a downward pointing gravity vector along the symmetry line on the tangent plane. Figure 7.5 shows the results on the evolving geometry, whereas Figure 7.6 allows a comparison of the same evolution law on a fixed surface. One clearly notices the impact of the surface evolution on the diffusion and advection process caused by the temporal variation of the angle of attack of the gravity force.

#### REFERENCES

- [1] M. BERTALMIÓ, F. MÉMILI, L. T. CHENG, G. SAPIRO, AND S. OSHER, *Geometric level set methods in imaging, vision, and graphics*, Springer, New York, 2003, ch. Variational Problems and Partial Differential Equations on Implicit Surfaces: Bye Bye Triangulated Surfaces?, pp. 381–397.
- [2] M. BURGER, *Finite element approximation of elliptic partial differential equations on implicit surfaces*, Computing and Visualization in Science, 12 (2009), pp. 87–100.
- [3] J. W. CAHN, P. FIFE, AND O. PENROSE, *A phase-field model for diffusion-induced grain-boundary motion*, Acta Materialia, 45 (1997), pp. 4397–4413.
- [4] D. A. CALHOUN, C. HELZEL, AND R. J. LEVEQUE, *Logically rectangular grids and finite volume methods for PDEs in circular and spherical domains*, 2008.
- [5] B. R. DE ARAÚJO AND J. A. P. JORGE, *Curvature dependent polygonization of implicit surfaces*, SIBGRAPI/SIACG, IEEE, (2004).
- [6] ———, *Adaptive polygonization of implicit surfaces*, Computers & Graphics, 29 (2005).
- [7] K. DECKELNICK, G. DZIUK, C. M. ELLIOTT, AND C. J. HEINE, *An h-narrow band finite element method for elliptic equations on implicit surfaces*, Preprint 18-07, Fakultät für Mathematik und Physik, Universität Freiburg, 2007.
- [8] QIANG DU AND LILI JU, *Finite volume methods on spheres and spherical centroidal Voronoi meshes*, SIAM J. Numer. Anal., 43 (2005), pp. 1673–1692.
- [9] QIANG DU AND DESHENG WANG, *Anisotropic centroidal Voronoi tessellations and their applications*, SIAM J. Sci. Comp., 26 (2005), pp. 737–761.

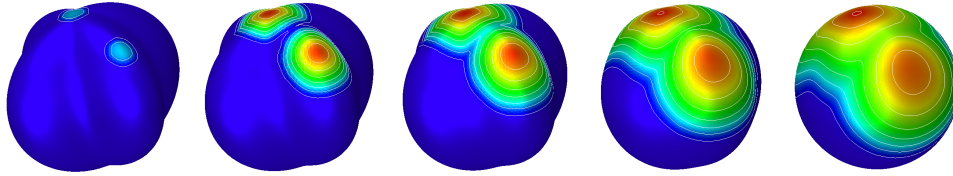


FIGURE 7.5. The evolution of a density governed by a diffusion and advection process on an evolving geometry with a localized source term is shown at different time steps. The underlying grid consists of 21960 triangles and 10982 vertices.

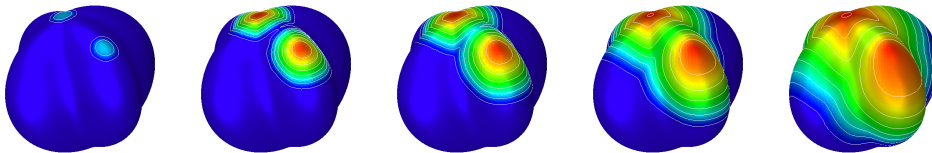


FIGURE 7.6. As in Figure 7.5 the evolution of a density under diffusion and advection by gravity is investigated. This time the underlying geometry is fixed.

- [10] G. DZIUK AND C. M. ELLIOTT, *Finite elements on evolving surfaces*, IMA J. Numer. Anal., 27 (2007), pp. 262–292.
- [11] G. DZIUK AND C. M. ELLIOTT, *Surface finite elements for parabolic equations.*, Journal of Computational Mathematics, 25 (2007), pp. 385–407.
- [12] B. ENGQUIST AND S. OSHER, *One-sided difference approximations for nonlinear conservation laws*, Math. Comp., 31 (1981), pp. 321–351.
- [13] R. EYMARD, T. GALLOUËT, AND R. HERBIN, *Finite volume methods*, in Handbook of numerical analysis, Vol. VII, North-Holland, Amsterdam, 2000, pp. 713–1020.
- [14] J. B. GREER, *An improvement of a recent Eulerian method for solving PDEs on general geometries*, J. Scientific Computing, 29, No. 3 (2006), pp. 321–352.
- [15] G. GRÜN, M. LENZ, AND M. RUMPF, *A finite volume scheme for surfactant driven thin film flow*, in Finite volumes for complex applications, III (Porquerolles, 2002), Hermes Sci. Publ., Paris, 2002, pp. 553–560.
- [16] I. HERRERA, R. E. EWING, M. A. CELIA, AND T. F. RUSSELL, *Eulerian-Lagrangian localized adjoint method for the advection-diffusion equation*, Adv. Water Resources, 13 (1990), pp. 187–206.
- [17] A. J. JAMES AND J. LOWENGRUB, *A surfactant-conserving volume-of-fluid method for interfacial flows with insoluble surfactant*, J. Comput. Phys., 201 (2004), pp. 685–722.
- [18] J. A. MACKENZIE AND W. R. MEKWI, *On the use of moving mesh methods to solve PDEs*, in Adaptive Computations: Theory and Algorithms, Science Press Beijing, 2007, pp. 243–278.
- [19] P.-O. PERSSON, *Mesh generation for implicit geometries*, PhD thesis, Massachusetts Institute of Technology, (2005).
- [20] R. V. ROY, A. J. ROBERTS, AND M. E. SIMPSON, *A lubrication model of coating flows over a curved substrate in space*, J. Fluid Mech., 454 (2002), pp. 235–261.
- [21] G. TURK, *Generating textures on arbitrary surfaces using reaction diffusion*, in Computer Graphics (SIGGRAPH), ACM Press, 1991, pp. 289–298.